Available online at www.sciencedirect.com
SCIENCE DIRECT®
Analytica Chimica Acta 494 (2003) 245–254
ANALYTICA CHIMICA ACTA
www.elsevier.com/locate/aca

# Use of X-ray and other techniques to analyse the phase transformation induced in archaeological cast iron after its stabilisation by the electrolytic method

M.L.A. Gil [a,*], A. Santos [b], M. Bethencourt [c], T. García [d], S. Fernández-Bastero [d], A. Velo [d], L. Gago-Duport [d]

[a] *Dpto. de Química Física, Universidad de Cádiz, 11510 Puerto Real, Cádiz, Spain*
[b] *Dpto. de Cristalografía y Mineralogía, Estrat., Geodca. y Petrol, y Geoqca, Universidad de Cádiz, 11510 Puerto Real, Cádiz, Spain*
[c] *Dpto. de Ciencia de los Materiales e Ingeniería Metalúrgica y Química Inorgánica, Universidad de Cádiz, 11510 Puerto Real, Cádiz, Spain*
[d] *Dpto. de Geociencias Marinas y Ord, Territorio, Universidad de Vigo, 36200 Vigo, Pontevedra, Spain*

Received 25 March 2003; received in revised form 22 July 2003; accepted 1 August 2003

**Abstract**

Electrolytic treatment at low currents intensities has been applied to a piece of cast iron, with the object of optimising a suitable methodology for the conservation of archaeological objects of iron. This technique has proved to be effective in the extraction of chloride from the structure of akaganeite (β-FeOOH($Cl_x$)), the principal corrosion product of iron in the marine medium.

The effectiveness of the electrolytic treatment has been proven by applying the Rietveld method to the patterns of X-ray powder diffraction of samples extracted from the corroded surface before and after treatment. This method has permitted the unequivocal determination of akaganeite by means of the deconvolution of the diffraction peaks overlapping those of other components of the sample. At the same time, the chemical composition of this non-stoichiometric iron oxyhydroxide has been determined. The presence or absence of chloride has been corroborated by means of scanning electron microscopy and energy dispersive X-ray spectroscopy. After the electrolytic treatment, akaganeite was not present in the sample. Thus, Rietveld analysis has been shown to be a very useful tool for monitoring the chloride extraction process, and for determining the presence of this oxyhydroxide of iron.
© 2003 Elsevier B.V. All rights reserved.

*Keywords:* Conservation, iron objects; Chlorides; X-ray diffraction; Rietveld analysis; Akaganeite

## 1. Introduction

Archaeological objects made of cast iron recovered from marine sites are characterised principally by thick concretions, with cathodic corrosion being the driving force of the process by which this concretion is formed [1]. Its origin is the biological colonization by marine organisms whose skeletal material constitutes the initial coarsening base. This layer, which is calcareous in nature, interacts with species of $Fe^{2+}$ and $Fe^{3+}$ in diffusion, originating from the underlying metal [2], thus producing chemical modifications in its composition. The result is a compact mineral casing adapted to the surface of the object.

Inside the concretion, the object undergoes a process of corrosion that transforms the iron into chemical

* Corresponding author. Tel.: +34-956016178; fax: +34-956016471.
*E-mail address:* almoraima.gil@uca.es (M.L.A. Gil).

0003-2670/$ – see front matter © 2003 Elsevier B.V. All rights reserved.
doi:10.1016/j.aca.2003.08.012

compounds distributed in uniform phases, from the remaining metallic nucleus out to the external graphitized zone composed of $H_2O$, FeO(OH), $SiO_2$, $Fe_3C$, iron chlorides, and graphite. The graphite forms an interlinked three-dimensional network that preserves the form of the original object [3]. The graphitised zone retains the appearance of the object, but has depleted the physical properties of the metal, converting it into an aggregate of mineral products. In function of the time of immersion and of the physico-chemical conditions of the surroundings, non-corroded or only partially corroded ferrite and perlite will be present in the nucleus of the metal, in sections contiguous to the graphitized zone [4].

Given that graphite is an electrical conductor, it provides a path for the electrons from the nucleus of the metal towards the external surface of the artefact. If this is partially dried in air, the components of the iron chloride decompose to form $Fe_2O_3$, $FeCl_3$, HCl and FeO(OH). This mixture of compounds provides almost ideal conditions for corrosion, and in the presence of atmospheric oxygen, this takes place very rapidly [5].

In environments with an excess of free chloride ions, these ions are incorporated into the first monolayer of some corrosion products. The process of total degradation is determined to a large extent by these $Cl^-$ present in the graphitized zone, in concentrations between 6 and 12 wt.% [3].

Therefore, the principal aim of any treatment of archaeological iron of marine origin is to eliminate chloride from the corrosion products. If this is done successfully, the development of the corrosion process due to chloride ceases and the rate of corrosion is reduced to more manegeable levels, where "conventional" methods against corrosion can operate efficiently.

An examination of different techniques for cleaning away chloride has shown that the limiting step in the release of these ions is their diffusion from the corrosion products. An increase of the velocity of diffusion of $Cl^-$ in corrosion products can be achieved by transforming the compounds of iron into other more dense compounds by reduction. Such reduction can be carried out by various means [6–10], electrolysis being one of the methods most commonly employed [11–13].

Basically, this functions as an electrolytic cell, consisting of a receptacle with a conducting solution or electrolyte, a cathode (the iron object) and an anode. The electrons required for the reaction are supplied by the application of an external voltage from an electrical source.

The application of low intensities of current minimizes the evolution of hydrogen on the cathode, which increases the rate of extraction of $Cl^-$ by increasing the area available for their diffusion [14]. Additionally, the employment of small currents enables the graphitized zone to be consolidated, due to the reduction of the iron oxyhydroxides of which it is composed, principally akaganeite, ($Fe^{3+}O(OH)(Cl_x)$), that is initially transformed into goethite ($\alpha$-FeO(OH)), and later into magnetite ($Fe_3O_4$ or $FeO{\cdot}Fe_2O_3$) [15]. This denser compound encourages the diffusion of chloride ions from the interior of the piece and consolidates the external metallic part, preventing subsequent oxidations.

This paper reports a study of the quantitative changes produced by the electrolytic method in the composition of a cast iron cannon ball, employing low current densities. Unlike other studies, the corrosion products of iron have been analysed structurally and mineralogically; this has permitted the analysis of the X-ray diffraction patterns to be used to check the extraction of chlorides, and to demonstrate the effectiveness of the electrolytic treatment.

The X-ray diffraction patterns have been analyzed using the Rietveld method [16,17]. This method overcomes the disadvantage involved in the use of such profiles in the primary analysis of the corrosion products of Fe [18], due to the overlapping of diffraction peaks presented by the various oxides and oxyhydroxides [19]; this overlapping constitutes a common characteristic of the polymineral pattern [20]. Therefore, this method has enabled each component to be determined unequivocally, as well as allowing a quantitative study to be made of these components before and after the treatment.

## 2. Experimental

### 2.1. Characteristics of the object

The object studied is a cannon ball, probably associated with the wreck of the San José, a vessel of the Philippines Armada sunk in 1619 after a storm in the Bay of Bolonia, Straits of Gibraltar (SW, Spain) [21].

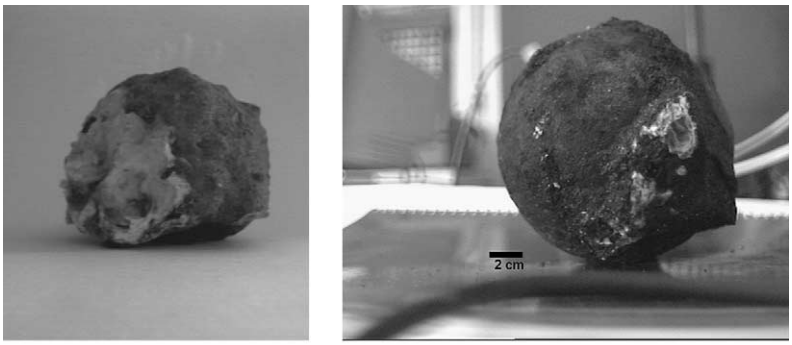


Fig. 1. Photographs of the ball with (a) and without (b) concretion.

After its recovery, the object was immediately immersed in a solution of 0.5 M NaOH. The total mass of the object was 1.6 kg, of which 0.4 kg corresponded to the calcareous concretion, which was eliminated mechanically. Its appearance and characteristics with and without the concretion can be seen in Fig. 1a and b, respectively. The thickness of this layer of concretion was 2 cm and the diameter of the cast iron cannon ball was 6 cm, with a film of corrosion products of 1 cm thickness. The original cannon ball was divided into four equal sections. To prevent contact with the electrolyte solution, the internal surfaces were protected with a film of Epofix Struer 40200029 resin.

### 2.2. Electrolytic treatment

The object was placed in an electrolytic cell as the cathode, surrounded by an anode of perforated aluminum to facilitate the circulation of the electrolyte, which consisted of a solution of 0.5 M NaOH. The voltage was supplied by a Silver Electronics EP-925 dc source. The range of potential on the cathode during the experiment remained between −0.94 and −0.88 V versus Ag/AgCl/KCl, these values falling within the immunity zone of the Pourbaix diagram.

The current of the cathode was maintained at approximately 50 μA by means of a resistor inserted between the current source and the cathode. The solution of the bath was renewed periodically so as to keep the concentration of chloride below 50 mg $ml^{-1}$. These conditions were maintained for 2 months, and the treatment was considered finished when the concentration of chloride in the solution remained below 50 ppm for 1 week.

### 2.3. Analysis of the samples

For the analysis of the components present in the samples, the X-ray powder diffraction (XRD) spectra were used; these were recorded by means of a Philips diffractometer with a graphite monochromator (Cu Kα), at 40 kV and 40 mA. The step-scan data were collected over the $2\theta$ angular range 3–80°, using a step size of 0.015 and a counting time of 2 s per step.

For the quantitative analysis of the different components of the X-ray diffraction spectra, the Rietveld method was employed, and for the treatment of the data obtained by this method, the original Fullprof program of Rodríguez-Carvajal et al. [22] has been utilized.

In comparison with conventional quantitative methods based on the calculation of the integrated intensities, the Rietveld method eliminates the errors associated with the overlapping of peaks and with the preferential orientation, since it is based on the analysis of the complete powder diffraction profile, in such a way that the experimental data can be fitted to a structural model [23].

In this method, the optimization procedure of a point-to-point fit by least squares minimizes the differences between the experimental values of the intensities and those calculated by the model. The fit between the experimental and calculated profiles is usually expressed in terms of the standard index of goodness (standard agreement indices). Notable among these is

the goodness of fit index (G of F), defined by Young et al. [24].

To obtain the calculated values, both the parameters associated with the crystalline structure of the minerals that comprise the diagram and the parameters associated with the diffraction spectrum (profile of reflections and background parameters) are utilized. In addition the abundance of each phase present in the sample is determined from scale factors that are obtained by refining the experimental diffractogram in function of the calculated profiles and of the background [25].

In this study, quantitative analyses have been made of all the minerals identified, together with refinements of the parameters of the profile and of the cell. In addition, in the case of the non-stoichiometric phases, the atomic coordinates and the factor of occupation were also refined. The goodness of the fit (G of F) was $<2$ in all the refinements.

The chemical composition of the metallic nucleus of the object was determined using a Spectrolab Jr model Spark Spectrometer, from Spectro. The microstructural characterization was performed with a Jeol 820-SM model scanning electron microscope, fitted with a LINK AN-10000 model energy dispersive spectrometer (EDS).

## 3. Results and discussion

### 3.1. Internal composition of the object

Table 1 shows the nominal composition of the nucleus of the ball before the electrolysis treatment, obtained by spark emission spectrometry.

The results of the analysis of the X-ray diffraction spectra are presented in Table 2 and in Fig. 2. These results show several components formed by α-Fe, cementite ($C_3Fe$) and quartz ($SiO_2$). The analysis following the Rietveld method has enabled the contribution, expressed in wt.% including associated standard deviation, of the three minerals to the total reflections present in the profile to be determined, and the specific contribution of some of the components to the intensity of the principal diffraction peak located at 2.03 Å ($2\theta = 44.62^\circ$). That maximum intensity is the result of the presence of α-Fe and of cementite in the sample, minerals that have a similar spacing (d). The fit made corresponds to the crystalline phases present in the profile. However, if Fig. 2 is analyzed in detail, two poorly defined peaks in the range of $2\theta$ around 4.5 and 18°, respectively, can be observed. The relatively limited resolution of the peaks demonstrates a scarcely crystalline phase and its fit involves a certain difficulty. Due to this, the percentages expressed in Table 2 should be considered as relative and approximate.

Table 1
Nominal composition of the nucleus of the ball before the electrolysis treatment, obtained by spark emission spectrometry

| Element | Percentage |
|---|---|
| Fe | 94.356 |
| Si | 0.267 |
| Mn | 0.110 |
| P | 0.014 |
| Cu | 0.002 |
| C | 5.251 |

Table 2
Mineral phases present in the interior of the ball before the electrolysis

| Bragg reflections | Mineral name | Compound | wt.% | S.D. |
|---|---|---|---|---|
| Phase 1 | Quartz | $SiO_2$ | 6.80 | 0.76 |
| Phase 2 | Cementite | $C_3Fe$ | 8.77 | 0.63 |
| Phase 3 | Alpha-iron | α-Fe | 84.43 | 0.13 |

This identification provides information about the principal elements (Fe, Si, C) present in the casting process during the manufacture of the cannon ball. The combination of these chemical elements explains the presence of the mineral phases previously mentioned.

The internal structure of the cannon ball corresponds to that of a grey casting iron, Fig. 3, showing flakes of graphite (dark lines) and perlite filling (cementite and α-Fe). Some parts of the graphite are combined with iron, forming cementite. These are the typical constituents of many historical casting irons [26,27] and are consistent with the composition determined by spark emission spectrometry and the analysis of the XRD patterns. This internal composition remains unaltered after the electrolysis.

The result of the metallographs in portions of the object before the electrolytic treatment is shown in Fig. 4. In this figure, films of primary graphite or type C graphite, also known as “foam graphite”, can be observed; these are characteristic of hypereutectic cast-

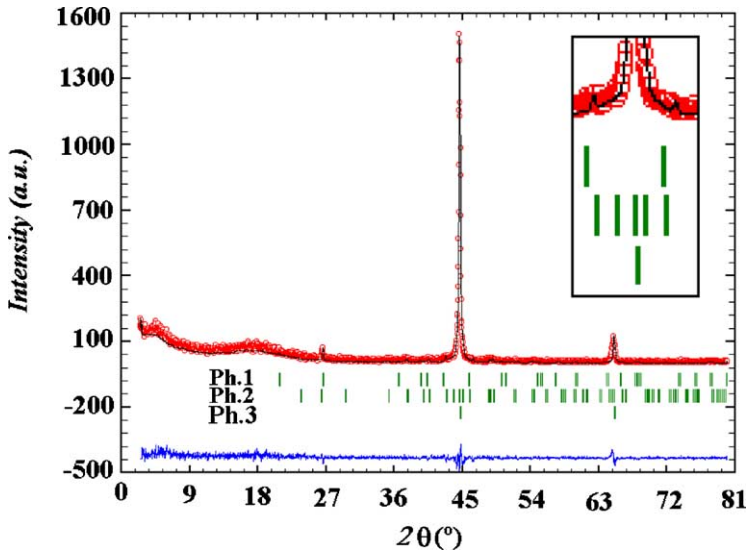


Fig. 2. Fit of the XRD-Rietveld phases of the internal composition before the electrolysis. The circles represent the experimental pattern of diffraction, and the continuous line the calculated pattern. The Bragg positions for the minerals involved are shown. Phase 1: quartz, phase 2: cementite, and phase 3: α-iron. The last curve represents the difference between the experimental and calculated diffraction patterns.

ings. It is termed "foam" because this type of graphite only appears during cooling, in the interval between the liquidus line and that of the eutectic, and since it is less dense than the iron, it tends to float.

This datum is confirmed by analyzing the chemical composition of the object. It can be observed that the content of carbon equivalent, %C + (%Si + %P/3), exceeds 4.3. In other words, considering the contribution not only of graphite, but also of silicon and phosphorus, the resulting casting is hypereutectic. In addition, the presence of a matrix of perlite (cementite and ferrite) is again observed in the metallographs.

### *3.2. Composition of the corroded surface of the object*

While the object has remained in the marine medium in contact with sediments, the surface has undergone a process of corrosion–concretion. Therefore, the analysis of the sample obtained from its external surface must reflect the presence of the minerals that constitute the sediments, as well as those minerals due to the process of corrosion–concretion.

Tables 3 and 4 show the results of the quantitative phase analysis, and the associated standard deviation, for each component, for the samples of the corroded surface taken before and after of the treatment. An example of the Rietveld fit corresponding to the components listed in Table 3 is presented in Fig. 5.

The characteristics of the analysis made with the Fullprof program enable the minerals present, as listed in this table, to be determined without ambiguity,

Table 3
Mineral phases of the corroded surface before the electrolysis

| Bragg reflections | Mineral name | Compound | wt.% | S.D. |
|---|---|---|---|---|
| Phase 1 | Quartz | $SiO_2$ | 45.30 | 0.36 |
| Phase 2 | Akaganeite | $Fe^{3+}O(OH)(Cl_{0.19})$ | 20.73 | 0.23 |
| Phase 3 | Magnetite | $Fe_2{}^{3+}Fe^{2+}O_4$ | 1.85 | 0.46 |
| Phase 4 | Plagioclase (albite) | $NaAlSi_3O_8$ | 18.46 | 0.29 |
| Phase 5 | Siderite | $Fe^{2+}CO_3$ | 13.66 | 0.22 |

Table 4
Mineral phases of the corroded surface after the electrolysis

| Bragg reflections | Mineral name | Compound | wt.% | S.D. |
|---|---|---|---|---|
| Phase 1 | Plagioclase (albite) | $NaAlSi_3O_8$ | 8.53 | 0.49 |
| Phase 2 | Goethite | $Fe^{3+}O(OH)$ | 9.19 | 0.37 |
| Phase 3 | Magnetite | $Fe_2{}^{3+}Fe^{2+}O_4$ | 23.23 | 0.37 |
| Phase 4 | Quartz | $SiO_2$ | 59.04 | 0.75 |

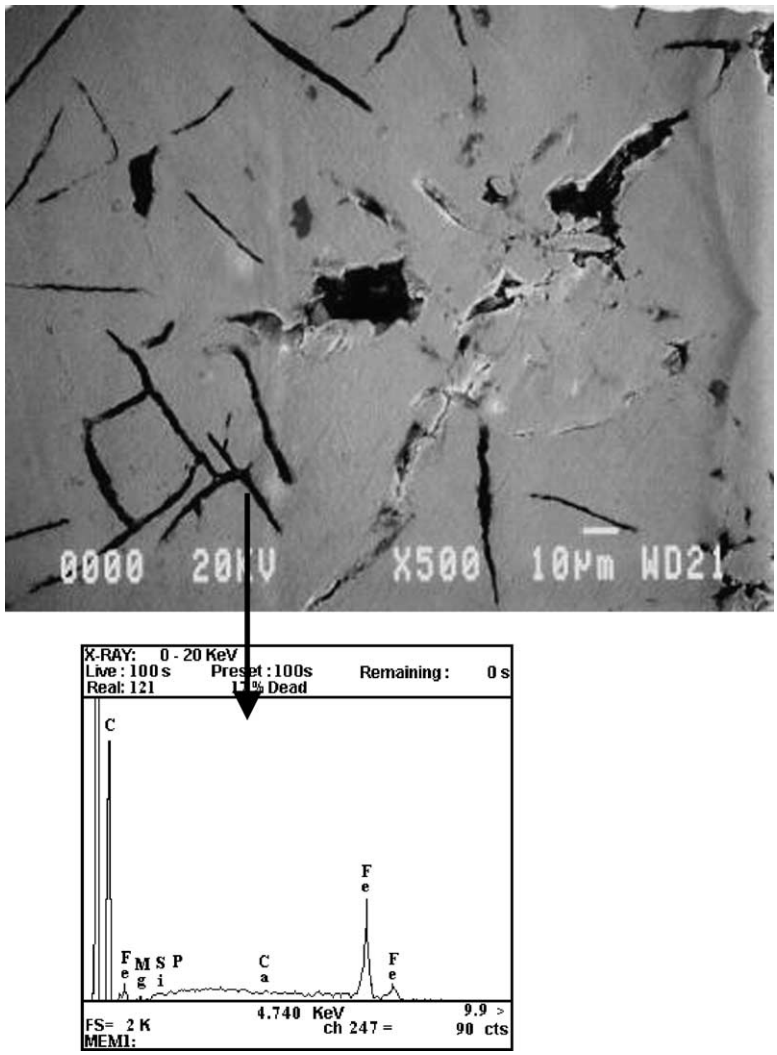


Fig. 3. SEM image of the interior of the cannon ball, showing flakes of graphite (dark lines) and perlite filling (cementite and α-Fe), and the corresponding EDS analysis.

despite the mutual overlapping of peaks that some of the minerals present. On this point, the most notable case is the presence of akaganeite and its contribution in the profile, for all those reflections specific to this mineral that are reflected by the wt.% value in Table 3. The intensity of the reflections located at 3.33 Å ($2\theta = 26.685^\circ$) and 2.54 Å ($2\theta = 35.18^\circ$) are the result of the contribution of akaganeite, as well as of the presence of quartz for the first peak and of magnetite for the second. Other components of the profile are siderite and plagioclase (albite). The fit of the profile, for the non-stoichiometric phases, has allowed us to refine the atomic coordinates and the factor of occupation. Table 5 gives these data for akaganeite, and its chemical composition.

The presence of all the components is not due to the same process of formation: akaganeite, $Fe^{3+}O(OH)(Cl_{0.19})$, is the oxyhydroxide of the β-phase of the iron, and is a corrosion product of iron in environments that contain chloride, normally observed in archaeological iron objects from marine sites. It has a crystalline structure of the hollandite

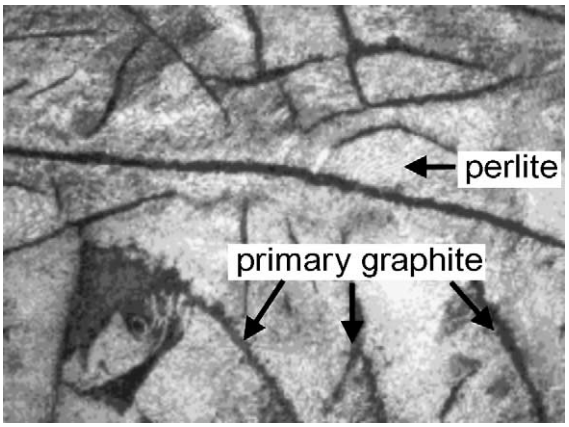


Fig. 4. Characteristic metallographs of a hypereutectic casting (400×).

type containing cavities of tubular appearance where the chloride ions reside [28]. These chloride ions are necessary for its formation and stabilization. The presence of this mineral has also been corroborated by means of SEM. In Fig. 6, one of the most frequent types of morphology in which this mineral is found [15] can be observed in the shape of the tip of a cigar. Also the chemical analysis by means of the corresponding EDS spectrum shows the presence of $Cl^-$ ions in its composition.

Other compounds are magnetite ($Fe_3O_4$ or $FeO{\cdot}Fe_2O_3$), an oxide where the iron has two states of oxidation, $Fe^{3+}$ and $Fe^{2+}$, and siderite ($FeCO_3$), iron(II) carbonate produced by anaerobic corrosion, by direct precipitation or involving sulphate reduction to $Fe^{2+}$. In this last case, the excess of $Fe^{2+}$ with respect to $SH^-$ in the presence of $HCO_3^-$ causes the precipitation of siderite. Both magnetite and siderite are products typical of the processes of corrosion during the formation of the concretions [1].

Quartz and plagioclase albite, $NaAlSi_3O_8$, are compounds present in marine sediments, the environment in which the ball has undergone the corrosion–concretion process.

After the electrolytic treatment, the phases present are shown in Table 4. Rietveld analysis distinguishes the presence of goethite, since this mineral presents reflections that overlap those of quartz. However, the most striking result is the absence of akaganeite. In Fig. 7, the appearance of the treated surface, as revealed by SEM, can be observed, together with the EDS spectrum that reflects the absence of chlorides in the sample.

This finding demonstrates how effective the electrolytic treatment is in the extraction of chloride; we can thus, interpret from this that the extraction of chloride causes the structural instability of the akaganeite.

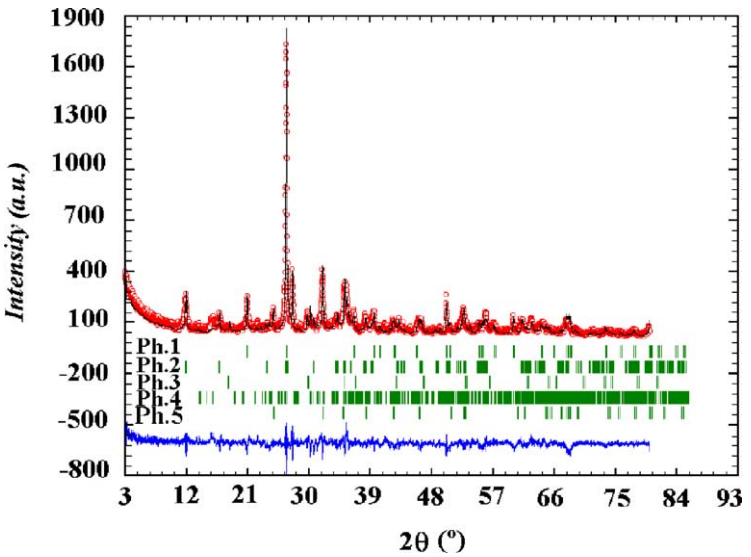


Fig. 5. Results of the XRD-Rietveld fit of the corroded surface before the electrolysis. Symbols are the same as in Fig. 2. Phase 1: quartz, phase 2: akaganeite, phase 3: magnetite, phase 4: plagioclase (albite), and phase 5: siderite.

Table 5
Parameters of the cell and of the profile (Akaganeite—$Fe^{3+}O(OH)(Cl_{0.19})$—space group $C2/M$[a])

| Atom | No. | Oxidation state | $x$ | $y$ | $z$ | $B$ | $S_0$ |
|---|---|---|---|---|---|---|---|
| Fe | 1 | +3 | 0.35969 | 0.00000 | 0.51393 | 0.00633 | 1.00000 |
| Fe | 2 | +3 | 0.14355 | 0.00000 | 0.79410 | 0.00633 | 1.00000 |
| O | 1 | −1 | 0.28090 | 0.00000 | 0.60579 | 0.01013 | 1.00000 |
| O | 2 | −1 | 0.35039 | 0.00000 | 0.30089 | 0.01013 | 1.00000 |
| O | 3 | −1 | 0.42827 | 0.00000 | 0.20182 | 0.01013 | 1.00000 |
| O | 4 | −1 | 0.21112 | 0.00000 | 0.14899 | 0.01013 | 1.00000 |
| Cl | 1 | −1 | 0.00000 | 0.00000 | 0.00000 | 0.02533 | 0.77354 |

Atomic coordinates and factor of occupation for the akaganeite non-stoichiometric phase.

[a] Cell parameters: $a = 14.8167$ Å; $b = 3.0308$ Å; $c = 10.5966$ Å; $\alpha = 90.0000°$; $\beta = 134.8074°$; $\gamma = 90.0000°$. Width parameters: $U = 0.00094$; $V = 0.00089$; $W = 0.00055$.

This finding can be deduced from the presence of goethite and magnetite in the XRD spectrum. On the one hand, the composition of goethite ($Fe^{3+}O(OH)$) corresponds to the same iron oxyhydroxide as akaganeite but with no chloride in its structure. Therefore, as a result of the treatment, a change has been induced both in the composition and in the structure of the oxyhydroxide, as described in the literature [27]. On the other hand, the increase in the content of magnetite is due to the conversion of akaganeite, in accordance

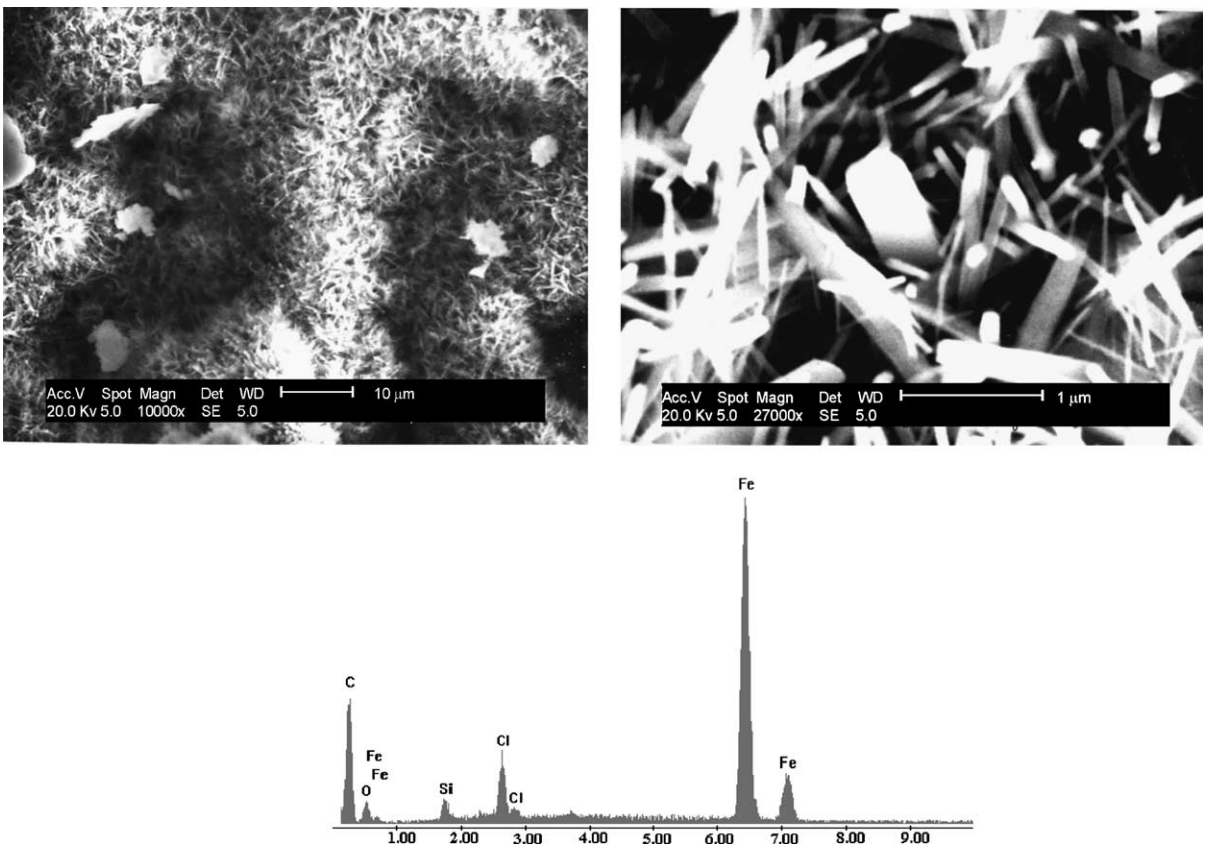


Fig. 6. SEM image of the corroded surface before the electrolysis, and the corresponding EDS analysis.

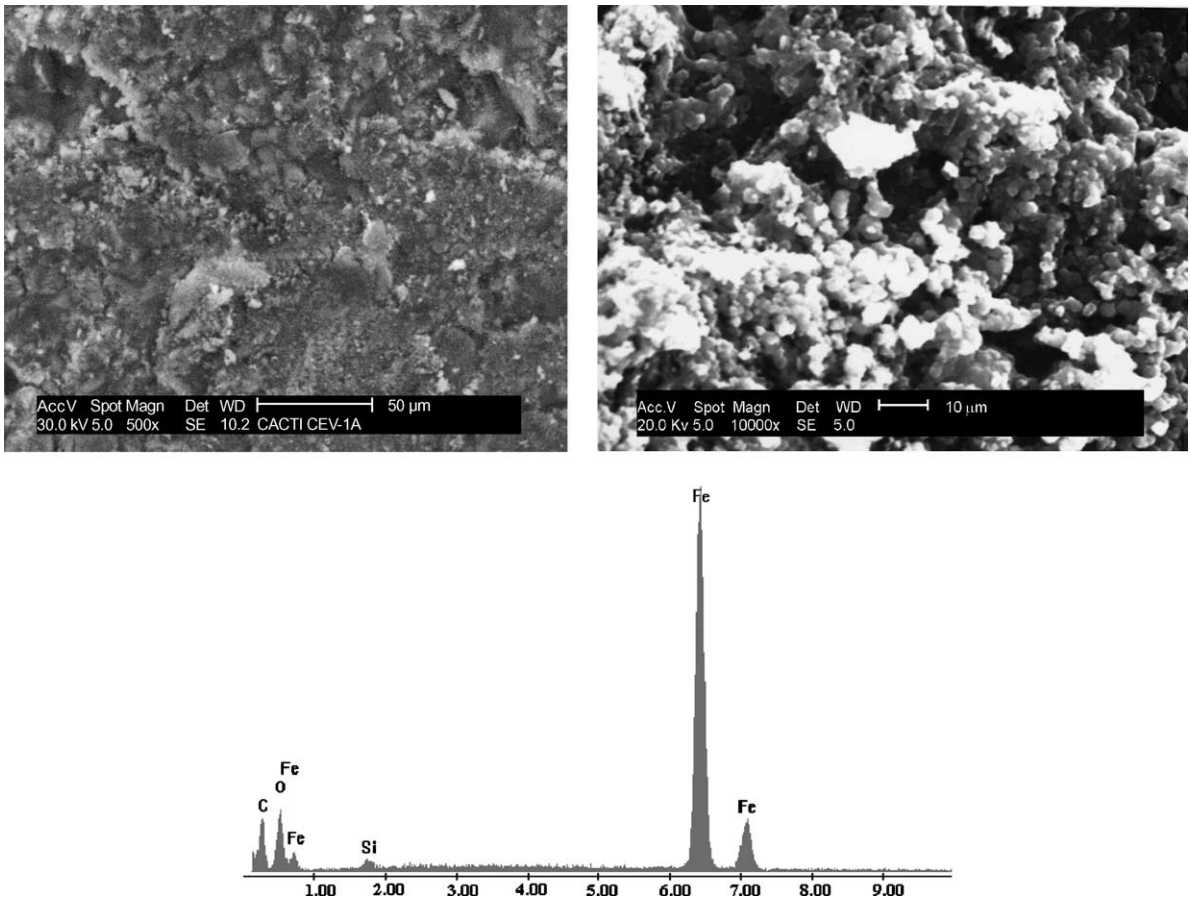


Fig. 7. SEM image of the corroded surface after the electrolysis, and the corresponding EDS analysis.

with the reduction reaction (I).

$$3FeO(OH) + H^+ + e^- \rightarrow Fe_3O_4 + 2H_2O \quad (1)$$

According to Pearson [29], this reaction leads to a decrease of the volume of approximately 1.7 $cm^3$ $mol^{-1}$ akaganeite. This increase in density will have facilitated the diffusion of chloride from the object to the solution during the electrolytic treatment.

The transformation reaction (I) has been fully described in the literature, with the presence of reducing agents [30,31] being an essential requirement. In our case, the reducing agent is the electrical potential, since the reducing action of NaOH at ambient temperature requires a very long period of time to take effect [15]. It has been described that the existence of akaganeite in the presence of chlorides is one of the reasons that explain the high content in magnetite of the corrosion products [32]. Finally, in Table 4, the absence of siderite in the X-ray profile is also notable. This absence can be explained taking into account the evolution of hydrogen on the cathode [33], since this phase is easily altered in the presence of protons.

## 4. Conclusions

The electrolytic method, applying low intensities of current, has been utilized to extract chloride ions from a cast iron cannon ball that had undergone a process of corrosion, submerged for several centuries at the bottom of the sea.

Using spark emission spectrometry, SEM, EDS and XRD to analyse the internal composition of the object, it was observed that this corresponded to α-Fe,

cementite and quartz, these being the mineral compounds of the principal elements (Fe, Si, C) present in the casting process during the manufacture of the cannon ball. This mineralogical composition remained unaltered after the treatment.

Rietveld analysis of the XRD patterns of the corroded surface before the treatment enabled the identification of akaganeite, by deconvolution of the highest intensity peak located at 3.33 Å ($2\theta = 26.685^{\circ}$). Additionally, the stoichiometry has been determined as that corresponding to akaganeite, $Fe^{3+}O(OH)(Cl_{0.19})$.

After treatment, the mineral phases containing iron present on the surface of the object are goethite and magnetite. From this finding, it is deduced that the electrolysis has produced the extraction of chloride from the piece, thus inducing the structural instability of the akaganeite and its disappearance. Therefore, Rietveld analysis of the XRD spectra is demonstrated to be a very useful tool for monitoring the electrolytic treatment, and thus determining the presence of akaganeite in the sample.

## Acknowledgements

This work was supported by the IAPH (Andalusian Institute for the Heritage Conservation) under Grant IAPH99-Hierro.

## References

[1] M.R. Al Agha, S.D. Burley, C.D. Curtis, J. Esson, J. Geol. Soc. 152 (1995) 157.
[2] N.A. North, Stud. Conserv. 27 (1982) 75.
[3] N.A. North, Conservation of Metals, Conservation of Marine Archaeological Objects, Butterworths, London, 1987, pp. 76–78.
[4] I.D. Macleod, J. Electroanal. Chem. 118 (1981) 291.
[5] N.A. North, Conservation of Metals, Conservation of Marine Archaeological Objects, Butterworths, London, 1987, pp. 145–147.
[6] H. Knight, Corrosion of Iron, Monograph, National Maritime Museum, London, 1982.
[7] A. Rinuy, F. Schewiezer, Stud. Conserv. 26 (1981) 29.
[8] N.A. North, C. Pearson, Stud. Conserv. 23 (1978) 174.
[9] H.J. Plenderheit, A.E.A. Werner, The Conservation of Antiquities and Works of Art, Oxford University Press, London, 1976.
[10] D. Watkinson, Chloride extraction from archaeological iron: comparative treatment efficiencies, Archaeological conservation and its consequences, in: Proceedings of the 16th International Congress, Copenhagen, 1996.
[11] D. Hamilton, Basic Methods of Conserving Underwater Archaeological Material Culture, US Department of Defense, Washington, 1996.
[12] R. Walker, Br. Corros. J. 31 (1996) 69.
[13] N.A. North, Electrolysis of marine iron, in: Proceedings of the Papers of First Southern Hemisphere Conference on Maritime Archaeology, Society of Oceans, Melbourne, 1977.
[14] W. Carlin, D. Keith, J. Rodriguez, Stud. Conserv. 46 (2001) 68.
[15] R.M. Cornell, R. Giovanoli, Clay Clay Miner. 38 (5) (1990) 469.
[16] H.M. Rietveld, Acta Crystall. 2 (1967) 151.
[17] H.M. Rietveld, J. App. Crystall. 2 (1969) 65.
[18] D.C. Cook, A.C. Van Orden, Corrosion, 2000.
[19] T. Fukasawa, M. Iwatsuki, M. Furukawa, Anal. Chim. Acta 281 (1993) 413.
[20] N.J. Elton, P.D. Salt, Anal. Chim. Acta 286 (1994) 37.
[21] D.C. Lakey, Shipwrecks in the Gulf of Cádiz, A catalog of historically documented wrecks from the fifteenth through the nineteenth centuries, Institute of Nautical Archaeology, 1987.
[22] J. Rodríguez-Carvajal, M. Anne, J. Parmentier, ILL Internal Report 87RO14T, Institute Laüe Langevin, Grenoble.
[23] W.G. Mumme, G. Tsambourakis, I.C. Madsen, R.J. Hill, Sedim. Res. J. 66 (1) (1996) 132.
[24] R.A. Young, E. Prince, R.A. Sparks, J. Appl. Cryst. 15 (1982) 357.
[25] R.L. Snyder, D.L. Bish, J.E. Post, D.L. Bish, Mineralogical Society of America, Washington, Rev. Mineral. 20 (1989) 101.
[26] R. Walker, Br. Corros. J. 31 (1) (1996) 70.
[27] B. Weckler, H.D. Lutz, Eur. J. Solid State Inorg. Chem. 35 (1998) 531.
[28] A.L. Mackay, Miner. Mag. 32 (1960) 547.
[29] C. Pearson, Conservation of Marine Archaeological Objects, Butterworths, London, 1987.
[30] N.A. North, C. Pearson, Alkaline sulfite reduction treatment of marine iron, ICOM, in: Proceedings of the Committee for Conservation at the 44th Triennial Meeting, Venice, 75/13/3, 1975, p. 1.
[31] N.A. North, M. Owens, Int. J. Naut. Arch. Und. Exp. 10 (1981) 95.
[32] T. Ishikawa, Y. Kondo, A. Yasukawa, K. Kandori, Corros. Sci. 40 (1998) 1239.
[33] T. Casanova, J. Crousier, Corros. Sci. 9 (1996) 1535.